Biophysical Journal Volume 109 November 2015 1978–1985

Article

Substrate Binding Specifically Modulates Domain Arrangements in Adenylate Kinase

Fabian Zeller[1] and Martin Zacharias[1,*]
[1]Physics Department, Technical University Munich, Garching, Germany

ABSTRACT The enzyme adenylate kinase (ADK) features two substrate binding domains that undergo large-scale motions during catalysis. In the apo state, the enzyme preferentially adopts a globally open state with accessible binding sites. Binding of two substrate molecules (AMP + ATP or ADP + ADP) results in a closed domain conformation, allowing efficient phosphoryl-transfer catalysis. We employed molecular dynamics simulations to systematically investigate how the individual domain motions are modulated by the binding of substrates. Two-dimensional free-energy landscapes were calculated along the opening of the two flexible lid domains for apo and holo ADK as well as for all single natural substrates bound to one of the two binding sites of ADK. The simulations reveal a strong dependence of the conformational ensembles on type and binding position of the bound substrates and a nonsymmetric behavior of the lid domains. Altogether, the ensembles suggest that, upon initial substrate binding to the corresponding lid site, the opposing lid is maintained open and accessible for subsequent substrate binding. In contrast, ATP binding to the AMP-lid induces global domain closing, preventing further substrate binding to the ATP-lid site. This might constitute a mechanism by which the enzyme avoids the formation of a stable but enzymatically unproductive state.

INTRODUCTION

Enzymes have developed elaborate strategies to efficiently catalyze reactions fundamental for cell function. As such, large-scale domain motions coupled to substrate binding are essential for the activity of a large number of enzymes (1). A prominent example is adenylate kinase (ADK), catalyzing the reversible interconversion of ATP-MG^{2+} + AMP and ADP-Mg^{2+} + ADP. The enzyme is involved in the regulation of energy homeostasis in bacteria and eukaryotic cells (2,3).

ADK possesses two binding cavities that are specifically occupied by AMP and ATP, or alternatively by two ADPs, in the functional states. The cavities are each formed by a large flexible domain termed AMP-lid and ATP-lid, in combination with the protein core. Several crystal structures of ADK have been determined, showing that these flexible domains can adopt an open conformation in the absence of substrates (4,5) and a closed conformation when substrates or inhibitors are bound (6-8) (see Fig. 1). In the closed conformation, active site residues and substrates are shielded from the aqueous environment and arranged in a configuration appropriate for the chemical reaction (11). The importance of the global domain rearrangements in the functional cycle has been emphasized by a study identifying the domain opening as the rate-limiting step for catalysis (12). However, despite being crucial for the biological activity of the enzyme, the mechanistic coupling between binding of different substrates and large-scale domain motion has not been fully understood.

Nuclear magnetic resonance (NMR) spectroscopy and fluorescence resonance energy transfer experiments indicate a high degree of conformational flexibility of ADK (5,13,14). Closing or partial closing of lids upon binding of the respective substrates has been observed (14-16). Evidence for different possible conformational substates is also given by crystallography. For example, a partially closed structure of an inactive variant of ADK in complex with an ATP analog has been determined that shows a closed ATP-lid and a fully opened AMP-lid (17). The question arises how, in detail, the domain motions and possible substates are modulated or induced by the binding of substrates to achieve efficient catalysis. As the substrates can potentially bind to different binding sites and to a broad ensemble of conformational states, accessibility of the pathways is substantially complicated.

In addition to the experiments, the dynamics of ADK and the possible influence of different substrates have been addressed in computational studies. Pathways between different conformations of apo ADK have been investigated making use of network models (18) or other non-atomistic models (19,20). Several atomistic continuous molecular dynamics (MD) simulations have been performed (21-24). However, such simulations are usually limited to timescales on which the domain rearrangements are rare events. Alternatively, coarse-grained models allow

Submitted August 3, 2015, and accepted for publication August 27, 2015.
*Correspondence: martin.zacharias@ph.tum.de
Editor: Amedeo Caflisch.

0006-3495/15/11/1978/8
http://dx.doi.org/10.1016/j.bpj.2015.08.049

more extensive sampling (20), but the accuracy of such models and the implicit treatment of the solvent may not be sufficient to analyze the influence of different substrates on the dynamics of ADK. More recently, progress has been made by employing advanced sampling methods in atomistic MD simulations on ADK (25-30). Significant contributions have emerged from these studies, but as they focused on ADK in the apo state or bound to an inhibitor, the dynamics in the presence of natural substrates have not been covered.

In this study, we employ atomistic MD simulations controlling substrate type and binding location to systematically expand the picture that has been outlined by experimental and previous simulation studies. Sampling of the domain configurations is achieved via umbrella-sampling simulations in combination with Hamiltonian replica exchanges. Using these sampling techniques, two-dimensional free-energy landscapes along the separate domain opening motions were calculated for apo ADK and nine different cases of bound natural substrates. These also include nonreactive states with substrates bound to the nondesignated lid domain. Each two-dimensional free-energy landscape is based on extensive sampling of >0.75 μs. The free-energy estimates from these MD simulations contribute insight into how evolution might have optimized the protein for its specific task, as they allow us to predict dominant features of binding and domain movement as well as to propose a mechanism that possibly avoids unproductive substrate bound states.

MATERIALS AND METHODS

Force field

The AMBER ff14SB force field (31) was used for the protein description. The TIP3P model (32) was used for the water molecules. The GAFF force field (33) in combination with Antechamber (34) was used to describe the AMP molecule. Specific force-field parameters were employed for ADP and ATP (35), the magnesium ion (36), and the potassium ions (37).

Starting structures

A total of 10 starting structures was prepared for *Escherichia coli* ADK: apo ADK, ADK in complex with two ADPs and Mg, and ADK with only one of the two binding sites occupied by AMP, ADP, ADP+Mg, or ATP+Mg. The closed ADK configuration was taken from a crystal structure of ADK in complex with the inhibitor AP5A (PDB: 1AKE (6)). For the simulations on apo ADK, the inhibitor was removed from the structure. To construct starting structures for the closed *E. coli* ADK in complex with natural substrates, the configuration of two ADP molecules and a magnesium ion bound to Mycobacterium tuberculosis ADK was taken from PDB: 2CDN (10). The AP5A inhibitor was replaced by this substrate configuration by least root-mean-square deviation (RMSD) fitting (9) the positions of the adenosine and adjacent phosphate groups of the ADP molecules onto the corresponding atom groups of AP5A (see Fig. 1). Redundant atoms were removed from the 2ADP+Mg complex in the cases of AMP, ADP and ADP+Mg, and an additional phosphate was added to ADP in the cases of ATP+Mg. The resulting 10 complexes were solvated with $\approx$8500 water molecules in a periodic octahedral box with edge length of $\approx$28 Å. The overall charge was neutralized by adding potassium ions. The starting structures were energy-minimized, heated up, and equilibrated for a total of 2 ns in the NTP ensemble, using AMBER14 (34) (see the Supporting Material for details).

Two-dimensional Hamiltonian replica-exchange umbrella-sampling simulations

All sampling simulations were performed in the NVT ensemble, using AMBER14. Details on the simulation parameters can be found in the Supporting Material. The opening coordinates were defined by the center-of-mass distances among the C_α atoms of residues 112–121,160–175, and 33–58 (AMP-lid), and of residues 1–28 and 125–152 (ATP-lid). Umbrella windows were set up with an intermediate spacing of 1 Å in both dimensions, between 20 Å and 31 Å for the AMP-lid opening and between 17 and 28 Å for ATP-lid opening distance. Based on the equilibrated structures, starting structures for the different umbrella windows were generated by successively applying the umbrella potentials with a force of 4 kcal/mol/Å^2 for 100 ps, first along the AMP-lid coordinate, then along the ATP-lid coordinate. A second set of starting structures was generated by repeating the process in the reverse order, starting from the previously obtained completely open structure. Positional restraints with a force of 0.025 kcal/mol/Å^2 were applied to the substrates during the generation of the initial umbrella window configurations to prevent dissociation due to the enforced fast domain motions. Sampling of the configurational space of two bound ligands in the case of 2ADP+Mg bound is considerably more demanding than sampling of only single bound substrates. To also incorporate states into the sampling in which the 2ADP+Mg complex is broken apart (a process that does not happen during affordable simulation times), before the generation of the second set of starting structures the ADP molecule bound to the AMP-lid site was driven to the open AMP-lid in the open ADK conformation. This was accomplished by applying an RMSD restraint of 1 kcal/mol/Å^2 on AMP-lid and the corresponding ADP molecule with respect to an open configuration from simulations of only ADP bound to the open AMP-lid for additional 20 ps. In the simulations of only ADP bound to the AMP-lid, this configuration occurred naturally. Finally, two strands of two-dimensional Hamiltonian replica-exchange umbrella-sampling (H-REMD-US) (38,39) simulations were performed in parallel, starting from the structures generated based on the closed and on the open state. During the sampling, no restraints besides the umbrella potentials were applied. Neighboring umbrella windows were allowed to exchange configurations every 1 ps according to the Metropolis criterion alternately within the strands and between the two strands. In this way, all umbrella simulations at the different positions and initiated from different structures were connected. The regions in the reaction coordinate plane corresponding to one closed and one open lid were omitted in the H-REMD-US runs to obtain a computationally advantageous number of 256 umbrella simulations, focusing sampling on the region of interest. During the sampling runs, the umbrella potential force was 2 kcal/mol/Å^2. Each window was sampled for 3 ns, corresponding to 6 ns of sampling for each umbrella window position, summing up to >0.75 μs of simulation time for each of the 10 ligation states. During the US simulations, the average internal RMSDs of the atom groups that defined the center-of-mass distances with respect to the starting structures measured <1.6 Å. Only at very open configurations did the AMP-Lid domain atom group reach a maximum internal RMSD value of 4.0 Å. This indicates that the center-of-mass distances are dominated by global domain arrangements and not by internal deformations. The rates of successful exchanges between the individual windows varied between 0.1 and 0.5. For the final potential of mean force (PMF) calculation via WHAM (40,41), the sampling data of the first of the 3 ns was

skipped as further equilibration. Convergence of the sampling was evaluated by calculating the PMFs for several subsets of the total sampling data. Details on the convergence of the sampling can be found in Figs. S1–S10. For the substrate RMSD calculations (34), the structures from all US trajectories were superimposed onto the starting structures with respect to the positions of all protein atoms (least RMSD fit). These structures were used to calculate the RMSD of all substrate atoms with respect to the starting structures. Figs. 1, 2, and 3 show the mean substrate RMSD values for 50 × 50 two-dimensional bins within the reaction coordinate plane.

RESULTS

Two-dimensional PMFs have been calculated along the center-of-mass distance between the mobile AMP-lid and ATP-lid domains and subsets of atoms of the protein core of *E. coli* ADK (Fig. 1). This allows an independent treatment of the movement of both domains and yields a two-dimensional free-energy projection in which the experimentally known open and closed ADK conformations are well-separated regions. The PMF calculations are based on H-REMD-US simulations, in which the sampling is distributed across the reaction coordinate plane by two-dimensional harmonic biasing potentials. In this way, the systems are driven into regions of phase space that might otherwise be rarely sampled. Unfavorable trapping of simulations in local free-energy minima is avoided by allowing configurations of neighboring windows to exchange according to a Monte Carlo scheme. Every umbrella window was seeded with starting configurations originating from a completely closed and a completely open configuration. This further enhances convergence of the sampling given that, due to the exchange scheme, the configurations can rapidly diffuse along the whole reaction coordinate space and reach an equilibrated distribution (see Materials and Methods).

Apo ADK and ADK fully occupied by 2ADP+Mg

In the absence of substrates the calculated free-energy landscape along the ADK domain opening coordinates (Fig. 1) indicates a broad minimum in the vicinity of the known experimental crystal structure conformation (*upper-right corner*). The broad free-energy basin allows considerable global motions of both lid domains toward the closed holo ADK conformation without significant changes in free energy. States with a single closed lid are disfavored only by a few kcal/mol. However, a state within few Å from the completely closed crystal structure configuration is disfavored by a free-energy penalty of ≈8 kcal/mol and hence hardly accessible. Analysis of the trajectories did not indicate significant rearrangements of the positively charged key residues in the apo form in comparison to the substrate bound form. During the simulations, the positively charged active sites remained partially hydrated also in the closed conformations (Fig. S11). Apparently, in absence of compensating negatively charged substrates, a complete closing of the lids creates a significant free-energy penalty due the electrostatic repulsion of the buried basic amino acids that surround the nucleotide binding sites.

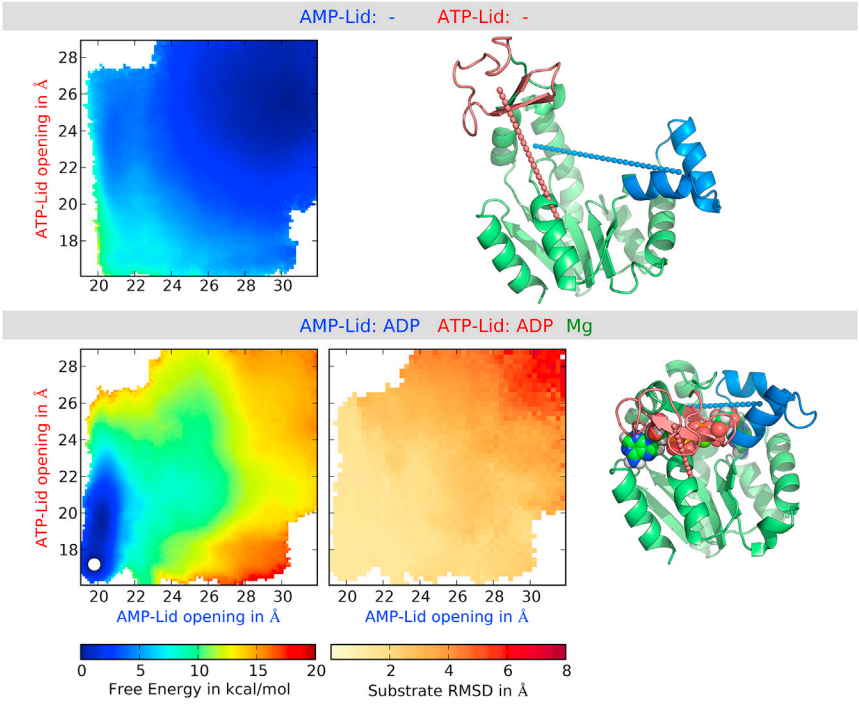

FIGURE 1 (*Left panels*) Two-dimensional free-energy landscapes along the opening of the AMP-lid and ATP-lid of ADK in the apo form (*top*) and in complex with 2ADP+Mg (*bottom*). (*Top-left* and *bottom-right regions* of the free-energy landscapes (*white regions in the plot*) were excluded from sampling; see Materials and Methods.) (*Middle panel*, *bottom*) For ADK in complex with 2ADP+Mg: the RMSD of the substrates, with respect to their configuration/position in the initial closed state of ADK for the different domain opening configurations during the simulations. (*Right panels*) Cartoon representations (9) corresponding to the crystal structures of apo ADK (PDB: 4AKE (4)) and fully occupied ADK (PDB: 1AKE (6)). AMP-lid (*blue*) and ATP-lid (*red*) residues and the corresponding opening coordinates (*dashed lines*). The original AP5A inhibitor of the closed *E. coli* Adenylate Kinase in PDB: 1AKE was replaced by two ADP molecules and a magnesium ion (*spheres*), taken from PDB: 2CDN (10) (see Materials and Methods). (*Circle*) The lid configuration corresponding to the crystal structure in the closed state is indicated in the PMF. The crystal structure configuration of open apo ADK is located at (30.9, 29.8). To see this figure in color, go online.

The calculated free-energy landscape in the presence of two ADP molecules and a magnesium ion located at the AMP and ATP binding sites predicts a global free-energy minimum coinciding with an experimental holo crystal structure (with a bound AP5A inhibitor). Indeed, NMR solution studies on *E. coli* ADK (14) but also crystal structures of ADK with two bound ADP molecules (8) indicate close similarity of inhibitor bound and double ADP bound closed ADK structures. Interestingly, a free-energy plateau can be observed for intermediate configurations. Only in the close vicinity of the global minimum complete closing is induced by a steep free-energy gradient, allowing initiation of the enzymatic reaction. Importantly, the simulations predict greater possible fluctuations and flexibility in the ATP-lid direction than in the AMP-lid direction. This is supported by recent crystal structures of ADK in complex with two ADP molecules (8), which in comparison to the AP5A-bound crystal structure show very similar arrangements of core and AMP-lid domain, but a slightly more open ATP-lid domain.

It should be noted that during the sampled timescales, the 2ADP+Mg complex stays close to the ADK closed form configuration (indicated by the small variation of the substrate RMSD with respect to its configuration in the closed form (Fig. 1)). In a realistic scenario, at a certain degree of domain opening, the substrate complex will eventually partly dissociate. The PMF for holo ADK therefore provides a good estimate of the free-energy landscape only in the vicinity of closed configurations.

Single site occupation of the ATP-lid by different substrates

Using the same H-REMD-US methodology, two-dimensional free-energy landscapes for the ADK domain motions were calculated for four different substrates (AMP, ADP, ADP+Mg, ATP+Mg) bound to the ATP-lid binding site (Fig. 2). Binding of AMP, ADP, or ADP+Mg does not result in drastic changes of the free-energy landscape in comparison to the apo form, only a shift of the ensembles toward more closed ATP-lid configurations and decreased lid-lid distances can be observed. Facilitation of AMP-lid closing is not indicated. The presence of Mg in the ADP case leads to a slightly more open ATP-lid ensemble. This is in line with the reported acceleration of lid opening upon addition of Mg (8).

In contrast, binding of ATP+Mg allows open and closed ATP-lid configurations and additionally influences the AMP-lid motion. A secondary free-energy minimum at a completely closed configuration can be identified. The free-energy basins around the minima are broad, indicating that the mobilities of the lids are maintained. These findings are strongly supported by a recent NMR study: upon binding of ATP to the ATP-lid, interconversion between open and closed ATP-lid states and an equilibrium between open and closed AMP-lid states with a slightly higher population of open states was observed (14).

Notably, ADP and ATP vary only slightly in position and orientation during ATP-lid opening and remain at the core part of the ATP binding site (Fig. 2, low substrate RMSD, *snapshots*). This finding coincides with a recent NMR study indicating initial binding of ATP to the core part of the ATP-binding site, not to the residues in the mobile ATP-lid domain (42). AMP, presumably due to the very low binding affinity to the ATP binding site ($K_d = 1.7$ mM (14)), exhibits significant mobility within the binding site upon domain opening (Fig. 2).

Single site occupation of the AMP-lid by different substrates

In another series of H-REMD-US simulations, the ADK domain motion upon binding of AMP, ADP, ADP+Mg, and ATP+Mg to the AMP-lid site was investigated (Fig. 3). For substrates binding to the AMP-lid, coupling to the ATP-lid dynamics can be observed. Binding of AMP to the AMP-lid results in a relatively flat domain opening free-energy landscape. The global minimum of the lid configurations is shifted toward the closed state, and the free-energy penalty to sample the completely closed state is significantly lowered in comparison with apo ADK. In NMR experiments, fluctuations between closed and open conformations upon binding of AMP to the AMP-lid were also reported (14). Partial closing of the ATP-lid was also observed in energy transfer experiments upon addition of AMP (15). Binding of ADP or ADP+Mg drastically changes the free-energy landscape, leading to a free-energy minimum at the closed state. The free-energy gradient along the AMP-lid coordinate is steeper, but also ATP-lid closing is favored. As in the ATP-lid site case, ADP+Mg leads to slightly more open configurations than ADP alone, again in line with faster lid opening (8). For ATP bound to the AMP-lid site, additionally, a strong tendency toward ATP-lid closing is indicated.

In contrast to the ATP-lid binding pocket, substrate arrangement in the AMP-lid pocket changes significantly upon domain opening. AMP and ADP remain attached to the AMP-lid and partially follow its opening movement (Fig. 3, *snapshots*). This is also shown by the increased substrate RMSD with respect to the equilibrated closed form configuration.

DISCUSSION

Despite many efforts in experimental and simulation studies, a full understanding of the global domain motion of ADK and its coupling to substrate binding is still lacking. In this study, free-energy landscapes, along with the changes in conformation of ADK for basically all possible ligation states with natural substrates and the apo form, have been

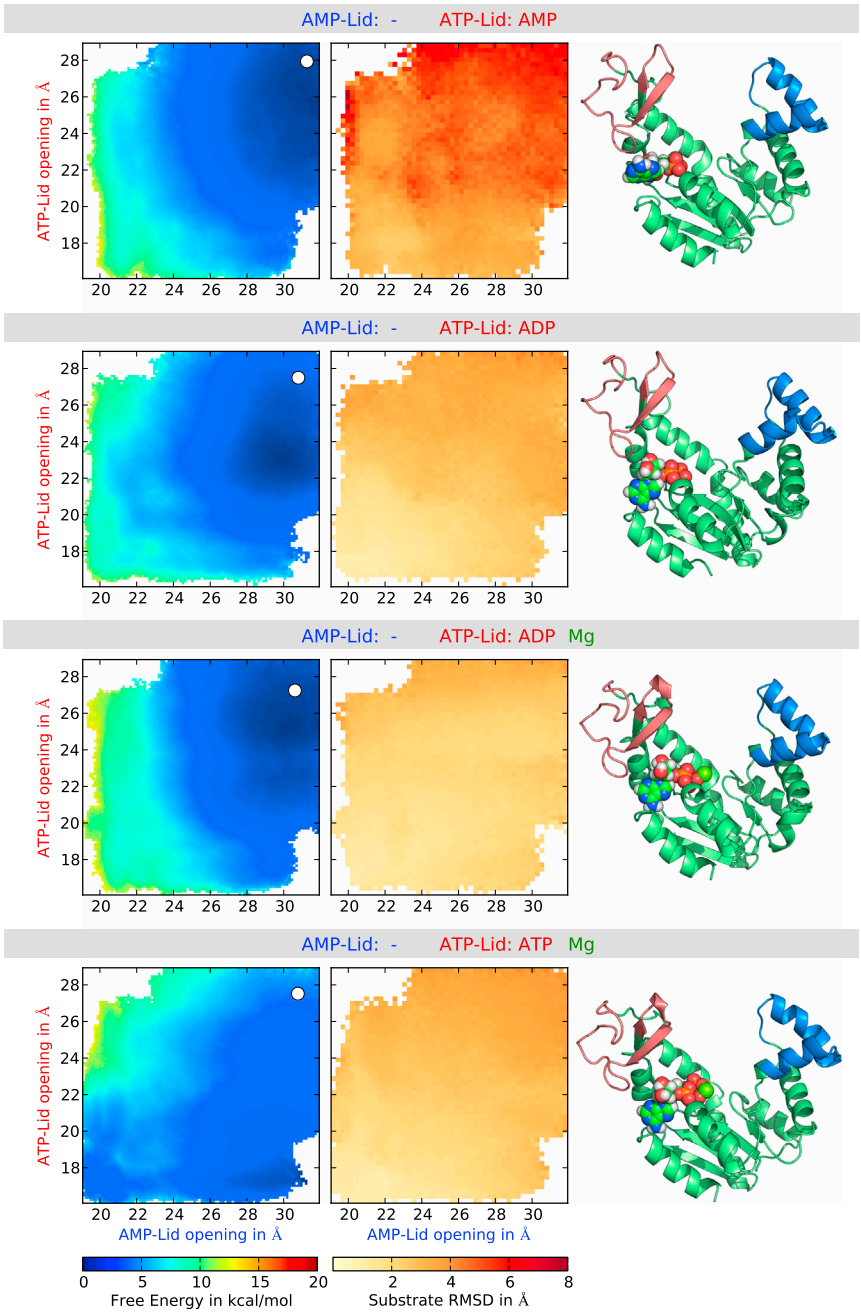

FIGURE 2 (*Left panels*) Two-dimensional free-energy landscapes along the opening of the AMP-lid and ATP-lid of ADK with AMP, ADP, ADP+Mg, or ATP+Mg bound to the ATP-lid binding site (see *panel title*). (*Middle panels*) Mean RMSD of the substrate with respect to its configuration in the initial closed state of ADK at the different domain opening configurations during the simulations. (*Right panels*) Exemplary snapshots from the sampled trajectories (*cartoon representation*) with the corresponding positions in the free energy plot indicated as circles. To see this figure in color, go online.

calculated. To adequately capture the conformational rearrangements, the two lid domains were controlled individually by means of two-dimensional US simulations. This comprehensive approach allows a systematic analysis of the interplay between substrate binding and lid motion. Significant differences in the free-energy landscapes were obtained for not only the apo and holo forms of ADK, but also for between the complexes that included only single substrates at the different binding sites.

The calculated two-dimensional PMF for apo ADK agrees qualitatively with experimental findings (12,13,17), which indicate a high degree of global flexibility and the possibility of adopting closed-like states even in the absence of substrates. However, our simulations indicate a significant free-energy barrier for adopting a completely closed state with both lid opening coordinates within a few Å from the crystal structure conformation of the holo enzyme. In particular, in fluorescence resonance energy transfer studies (13), closing of ADK in the absence of substrate or inhibitors was observed. It is, however, not clear if the experimental spatial resolution is indeed sufficient to distinguish completely closed states from closed-like states that do not significantly differ in hydration of the polar and charged residues near the substrate binding sites. The

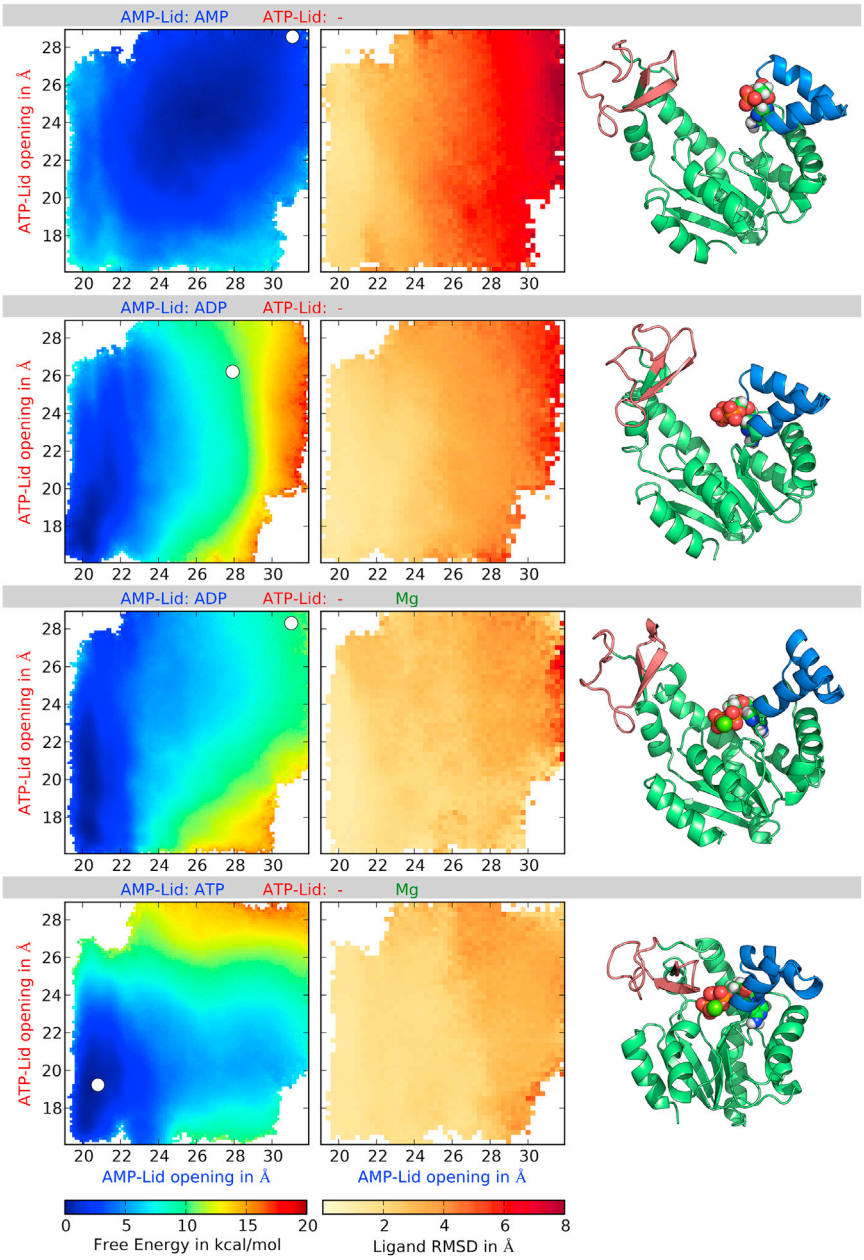

FIGURE 3 (*Left panels*) Two-dimensional free-energy landscapes along the opening of the AMP-lid and ATP-lid of ADK with AMP, ADP, ADP+Mg, or ATP+Mg bound to the AMP-lid binding site. (*Middle panels*) Mean RMSD of the substrate with respect to its configuration in the initial closed state of ADK at the different domain opening configurations during the simulations. (*Right panels*) Exemplary snapshots from the sampled trajectories (*cartoon representation*) with the corresponding positions in the free energy plot indicated as circles. To see this figure in color, go online.

calculated free-energy landscape for the apo form argues against a pure conformational selection mechanism for substrate binding. This is also supported by NMR studies on single substrate binding to ADK (42). Previous MD simulation studies that were either based on an implicit solvation model (26) or performed in explicit solvent also predicted a significant penalty for complete closing in the apo form (22,30). The simulations on holo ADK suggest that opening of the ATP-lid is the most likely first step in the release of the substrates (or products), as the free-energy landscape indicates a higher mobility of the ATP-lid compared to the AMP-lid in the holo form. Because domain opening is the rate-limiting step for catalysis (12), it appears reasonable that the opening motion of one of the lids in the holo state is not disfavored by a steep free-energy gradient.

Strikingly, the free-energy landscapes for single substrate bound states of ADK strongly depend on the type and position of the substrate. For all single substrate bound states for which, to our knowledge, experimental data is available, the free-energy landscapes are compatible with the experimental findings (see Results). In general, we observe that upon binding of a substrate to its corresponding lid (which can initiate an enzymatically productive occupation state of ADK), flexibility of the opposing lid is maintained with significant population of open configurations. In this way, efficient binding of the second substrate can be achieved that, in a closed state, would be sterically hindered.

Of special interest is the possible binding of substrates to the nondesignated lid. Presumably, binding of AMP to the ATP-lid binding site is of little relevance because AMP binds to the ATP binding site only weakly compared to ATP (K_D (AMP) = 1700 μM versus K_D (ATP) = 50 μM (14)). In line with this weak binding, in our simulations the AMP molecule showed large mobility in the ATP-lid site. However, the situation is different for binding of ATP to the AMP binding site. A significant fraction of ADK molecules may bind ATP in the incorrect binding site under equilibrium conditions (K_D (ATP) = 750 μM versus K_D (AMP) = 210 μM (42)). Note that this case is difficult to access (or isolate) experimentally because, once the ATP-binding site is occupied, binding of a second ATP to the AMP site is not possible for sterical reasons. In contrast to the productive initiation states, ATP bound incorrectly to the AMP-lid site results in closing and restricted mobility of both the AMP-lid and the ATP-lid. The closing of both lids may prevent binding of a second incoming nucleotide to the ATP-lid site, which would result in a stable but unproductive blocking state. Some possible processes, after initial binding of ATP+Mg (which has a much higher physiological concentration than ADP or AMP (43)) to each of the lids, are exemplified in Fig. 4.

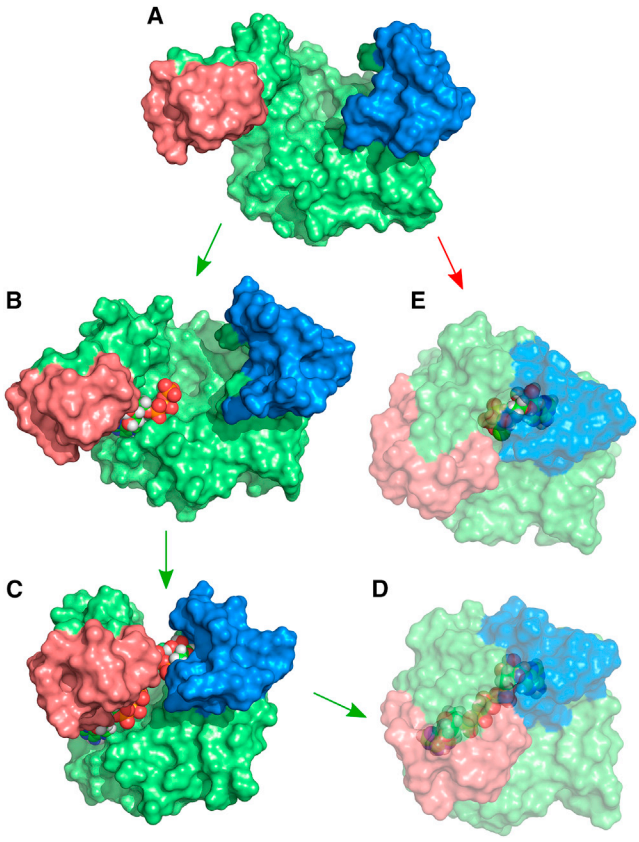

FIGURE 4 Schematic illustration of possible pathways initiated by ATP+Mg binding on the basis of ADK configurations obtained from the simulations. (*A*) Open, flexible ADK without substrates. (*B*) Upon binding of ATP+Mg to the ATP-lid site, flexibility of both lids is maintained. The AMP-lid is most probably found in open states. (*C*) AMP (added to the figure) can bind to the open AMP-lid. (*D*) Once two adequate substrates are bound, complete binding is induced, thereby facilitating the chemical reaction. (*E*) Binding of ATP+Mg to the AMP-lid site induces a global shift to closed conformations. This may hinder further occupation of the ATP-lid site, which would result in a stable but unproductive state. To see this figure in color, go online.

More generally, we observe that the lid behavior is intrinsically asymmetric. While for the ATP-lid, the substrates appear to bind with a high fraction of their affinity to the open state and only slightly promote lid closing, the same substrates induce a considerable stronger tendency toward closing when bound to the AMP-lid. Given that the ATP+AMP bound state is asymmetric, it appears necessary that an enzyme that needs to distinguish such states evolves asymmetric binding site lids. Additionally, providing a stable initiation state in the form of an open ATP-lid might be beneficial for the overall catalysis rate.

The simulations indicate that ADK has evolved in a way that initial substrate binding corresponding to productive occupation states still maintains the opposing lid open and accessible for the subsequent substrate. Such a behavior could hardly be realized with only one movable lid. Furthermore, incorrect single substrate bound states might be hindered from moving toward stable but unproductive fully occupied states by closing of both lids, sterically preventing further occupation. For enzymes like ADK, this strategy might be necessary because considerable binding affinity for unproductive initial occupation states cannot always be avoided by the composition of the binding sites due to the structural similarity of the substrates.

SUPPORTING MATERIAL

Supporting Materials and Methods and eleven figures are available at http://www.biophysj.org/biophysj/supplemental/S0006-3495(15)00938-8.

AUTHOR CONTRIBUTIONS

F.Z. performed research, analyzed data, and wrote the article; and M.Z. designed research and wrote the article.

ACKNOWLEDGMENTS

We thank Benjamin Pelz, Gabriel Zodiak, and Matthias Rief for helpful discussions.

This work was supported by the Deutsche Forschungsgemeinschaft (grant No. SFB1035/B02). Support of the Leibnitz Rechenzentrum Super Computer Center providing computer time within grant No. pr84ko is gratefully acknowledged.

REFERENCES

1. Hammes, G. G. 2002. Multiple conformational changes in enzyme catalysis. *Biochemistry.* 41:8221–8228.

2. Dzeja, P., and A. Terzic. 2009. Adenylate kinase and AMP signaling networks: metabolic monitoring, signal communication and body energy sensing. *Int. J. Mol. Sci.* 10:1729–1772.
3. Knowles, J. R. 1980. Enzyme-catalyzed phosphoryl transfer reactions. *Annu. Rev.* 49:877–919.
4. Müller, C. W., G. J. Schlauderer, …, G. E. Schulz. 1996. Adenylate kinase motions during catalysis: an energetic counterweight balancing substrate binding. *Structure.* 4:147–156.
5. Henzler-Wildman, K. A., V. Thai, …, D. Kern. 2007. Intrinsic motions along an enzymatic reaction trajectory. *Nature.* 450:838–844.
6. Müller, C. W., and G. E. Schulz. 1992. Structure of the complex between adenylate kinase from *Escherichia coli* and the inhibitor Ap5A refined at 1.9 Å resolution. A model for a catalytic transition state. *J. Mol. Biol.* 224:159–177.
7. Abele, U., and G. E. Schulz. 1995. High-resolution structures of adenylate kinase from yeast ligated with inhibitor Ap5A, showing the pathway of phosphoryl transfer. *Protein Sci.* 4:1262–1271.
8. Kerns, S. J., R. V. Agafonov, …, D. Kern. 2015. The energy landscape of adenylate kinase during catalysis. *Nat. Struct. Mol. Biol.* 22:124–131.
9. Schrödinger, LLC. 2010. The PyMOL Molecular Graphics System, Ver. 1.7.4. www.pymol.org.
10. Bellinzoni, M., A. Haouz, …, P. M. Alzari. 2006. The crystal structure of mycobacterium tuberculosis adenylate kinase in complex with two molecules of ADP and Mg^{2+} supports an associative mechanism for phosphoryl transfer. *Protein Sci.* 15:1489–1493.
11. Schulz, G. E. 1992. Induced-fit movements in adenylate kinases. *Faraday Discuss.* 93:85–93.
12. Wolf-Watz, M., V. Thai, …, D. Kern. 2004. Linkage between dynamics and catalysis in a thermophilic-mesophilic enzyme pair. *Nat. Struct. Mol. Biol.* 11:945–949.
13. Hanson, J. A., K. Duderstadt, …, H. Yang. 2007. Illuminating the mechanistic roles of enzyme conformational dynamics. *Proc. Natl. Acad. Sci. USA.* 104:18055–18060.
14. Adén, J., and M. Wolf-Watz. 2007. NMR identification of transient complexes critical to adenylate kinase catalysis. *J. Am. Chem. Soc.* 129:14003–14012.
15. Bilderback, T., T. Fulmer, …, M. Glaser. 1996. Substrate binding causes movement in the ATP binding domain of *Escherichia coli* adenylate kinase. *Biochemistry.* 35:6100–6106.
16. Sinev, M. A., E. V. Sineva, …, E. Haas. 1996. Domain closure in adenylate kinase. *Biochemistry.* 35:6425–6437.
17. Schlauderer, G. J., K. Proba, and G. E. Schulz. 1996. Structure of a mutant adenylate kinase ligated with an ATP-analogue showing domain closure over ATP. *J. Mol. Biol.* 256:223–227.
18. Maragakis, P., and M. Karplus. 2005. Large amplitude conformational change in proteins explored with a plastic network model: adenylate kinase. *J. Mol. Biol.* 352:807–822.
19. Whitford, P. C., S. Gosavi, and J. N. Onuchic. 2008. Conformational transitions in adenylate kinase. Allosteric communication reduces misligation. *J. Biol. Chem.* 283:2042–2048.
20. Bhatt, D., and D. M. Zuckerman. 2010. Heterogeneous path ensembles for conformational transitions in semi-atomistic models of adenylate kinase. *J. Chem. Theory Comput.* 6:3527–3539.
21. Ping, J., P. Hao, …, J. F. Wang. 2013. Molecular dynamics studies on the conformational transitions of adenylate kinase: a computational evidence for the conformational selection mechanism. *BioMed Res. Int.* 2013:628536.
22. Song, H. D., and F. Zhu. 2013. Conformational dynamics of a ligand-free adenylate kinase. *PLoS One.* 8:e68023.
23. Brokaw, J. B., and J. W. Chu. 2010. On the roles of substrate binding and hinge unfolding in conformational changes of adenylate kinase. *Biophys. J.* 99:3420–3429.
24. Pontiggia, F., A. Zen, and C. Micheletti. 2008. Small- and large-scale conformational changes of adenylate kinase: a molecular dynamics study of the subdomain motion and mechanics. *Biophys. J.* 95:5901–5912.
25. Lou, H., and R. I. Cukier. 2006. Molecular dynamics of apo-adenylate kinase: a principal component analysis. *J. Phys. Chem. B.* 110:12796–12808.
26. Arora, K., and C. L. Brooks, 3rd. 2007. Large-scale allosteric conformational transitions of adenylate kinase appear to involve a population-shift mechanism. *Proc. Natl. Acad. Sci. USA.* 104:18496–18501.
27. Potoyan, D. A., P. I. Zhuravlev, and G. A. Papoian. 2012. Computing free energy of a large-scale allosteric transition in adenylate kinase using all atom explicit solvent simulations. *J. Phys. Chem. B.* 116:1709–1715.
28. Wang, J., Q. Shao, …, W. Zhu. 2014. Exploring transition pathway and free-energy profile of large-scale protein conformational change by combining normal mode analysis and umbrella sampling molecular dynamics. *J. Phys. Chem. B.* 118:134–143.
29. Matsunaga, Y., H. Fujisaki, …, A. Kidera. 2012. Minimum free energy path of ligand-induced transition in adenylate kinase. *PLOS Comput. Biol.* 8:e1002555.
30. Formoso, E., V. Limongelli, and M. Parrinello. 2015. Energetics and structural characterization of the large-scale functional motion of adenylate kinase. *Sci. Rep.* 5:8425.
31. Hornak, V., R. Abel, …, C. Simmerling. 2006. Comparison of multiple AMBER force fields and development of improved protein backbone parameters. *Proteins.* 65:712–725.
32. Jorgensen, W. L., J. Chandrasekhar, …, M. L. Klein. 1983. Comparison of simple potential functions for simulating liquid water. *J. Chem. Phys.* 79:926–935.
33. Wang, J., R. M. Wolf, …, D. A. Case. 2004. Development and testing of a general AMBER force field. *J. Comput. Chem.* 25:1157–1174.
34. Case, D., J. T. Berryman, …, P. Kollman. 2015. AMBER 2015. University of California at San Francisco, San Francisco, CA.
35. Meagher, K. L., L. T. Redman, and H. A. Carlson. 2003. Development of polyphosphate parameters for use with the AMBER force field. *J. Comput. Chem.* 24:1016–1025.
36. Allnér, O., L. Nilsson, and A. Villa. 2012. Magnesium ion-water coordination and exchange in biomolecular simulations. *J. Chem. Theory Comput.* 8:1493–1502.
37. Joung, I. S., and T. E. Cheatham, 3rd. 2008. Determination of alkali and halide monovalent ion parameters for use in explicitly solvated biomolecular simulations. *J. Phys. Chem. B.* 112:9020–9041.
38. Torrie, G. M., and J. P. Valleau. 1977. Nonphysical sampling distributions in Monte Carlo free-energy estimation: Umbrella sampling. *J. Comput. Phys.* 23:187–199.
39. Fukunishi, H., O. Watanabe, and S. Takada. 2002. On the Hamiltonian replica exchange method for efficient sampling of biomolecular systems: application to protein structure prediction. *J. Chem. Phys.* 116:9058.
40. Kumar, S., J. M. Rosenberg, …, P. A. Kollman. 1992. The weighted histogram analysis method for free-energy calculations on biomolecules. I. The method. *J. Comput. Chem.* 13:1011–1021.
41. Grossfield, A. 2013. WHAM: the weighted histogram analysis method, Ver. 2.0.7. http://membrane.urmc.rochester.edu/content/wham.
42. Ådén, J., C. F. Weise, …, M. Wolf-Watz. 2013. Structural topology and activation of an initial adenylate kinase-substrate complex. *Biochemistry.* 52:1055–1061.
43. Beis, I., and E. A. Newsholme. 1975. The contents of adenine nucleotides, phosphagens and some glycolytic intermediates in resting muscles from vertebrates and invertebrates. *Biochem. J.* 152:23–32.